arXiv:1512.06990v2 [cond-mat.soft] 7 Jun 2016

Polymer Adsorption on Curved Surfaces

Handan Arkın[1, 2, *] and Wolfhard Janke[1, †]

[1] *Institut für Theoretische Physik, Universität Leipzig, Postfach 100 920, D-04009 Leipzig, Germany*
[2] *Department of Physics Engineering, Faculty of Engineering, Ankara University, Tandogan, 06100 Ankara, Turkey*

The conformational behavior of a coarse-grained semiflexible finite polymer chain near an attractive spherical surface was investigated by means of generalized-ensemble Monte Carlo computer simulations. In a detailed analysis of canonical equilibrium data over a wide range of sphere radius and temperature, we have constructed the phase diagrams both for non-grafted and end-grafted polymers. Phase diagrams are discussed for both cases and compared with each other.

I. INTRODUCTION

The interaction of macromolecules with differently shaped substrates is particularly important for interdisciplinary research and nano-technological applications including, e.g., the fabrication of biosensors [1] and peptide adhesion [2] to metals [3, 4] or semiconductors [5–7]. The knowledge of structure formation for a variety of interfaces has therefore been a challenging subject of numerous experimental and computational studies. This includes thermodynamic studies of polymers at planar surfaces [8–24], and also under pulling force [25, 26], and also at curved surfaces such as nanotubes, nano-strings and nano-particles [27–31]. Polymer adsorption on flat surfaces plays an important role within a wide perspective. Due to many possible applications, these hybrid systems have been extensively studied from all aspects. The understanding of the conformational properties of a polymer requires systematic studies because of the cooperative effect of the monomers in response to different system conditions. The geometric effect of an attractive substrate results in a rich phase behavior caused by the competition between monomer-monomer and monomer-surface interaction. By combining Monte Carlo simulations with atomistic, coarse-grained and continuum models, many studies have been done to investigate nano-particle–polymer interactions for different geometries, such as cylinder and sphere [32]. Tanaka *et al.* [33] examined the freezing transition of compact polyampholytes, for both single and multiple chains. There has been a number of studies of these systems to determine the effects of surface charge densities [34] and solvent conditions on the morphologies of polymer chains. Recently, employing a single-chain mean-field theory for polymers grafted to a flat surface has featured different morphologies for which, by controlling the self-assembly conditions, non-aggregated chains can coexist with micelles [35]. Using computer simulations, Barr and Panagiotopoulos [36] studied a system of polymers grafted to a spherical nano-particle in salt solution to gain insight into the conformational behavior of polymers on curved surfaces. Silver nano-particles have also been considered experimentally as catalyst for enhanced amyloid peptide fibrillation [37, 38].

Recently we have investigated the purely steric confinement effect of a steric spherical cage with a simple flexible polymer chain to find the influence on the location of the collapse and freezing transitions [39]. Another hybrid system under consideration was a polymer chain inside an attractive spherical cage for which we have constructed the finite-temperature phase diagram depending on the attraction strength of the sphere inner wall and the temperature [40, 41] and investigated the ground-state properties [42]. We have also compared the results with the attractive flat surface [43]. These systems exhibit a rich phase behavior ranging from highly ordered, compact to extended, random coil structures.

Here, we consider the opposite situation: A nano-sphere whose attractive outer spherical surface is the target for the adsorbing polymer. This problem could have practical implications for a broad variety of applications ranging from protein-ligand binding, designing smart sensors to molecular pattern recognition [44–47] and for the discovery of new drugs that bind to specific receptors. Therefore it is interesting to study the adsorption of macromolecules on different types of substrates and identify the conformational changes that a polymer can experience at the interface. In this paper, we are going to investigate a simple coarse-grained polymer model interacting with a spherical surface of varying curvature by means of generalized-ensemble Monte Carlo computer simulations. This method enables us to describe the different phases of the finite chain over a wide range of sphere radius and temperature. In a comparative

*E-mail: Handan.Olgar@eng.ankara.edu.tr
†E-mail: Wolfhard.Janke@itp.uni-leipzig.de;
Homepage: http://www.physik.uni-leipzig.de/CQT.html

study, we shall discuss how the structural phase diagram changes with the sphere radius and temperature, both for non-grafted and end-grafted polymer chains.

The rest of the paper is organized as follows. In Section II the model system is described in detail. Then, in Section III the multicanonical Monte Carlo simulation method is reviewed shortly and the measured observables are introduced. Section IV presents and discusses the main results, the phase diagrams for the two systems under consideration. Finally, Section V concludes the paper with a summary of our findings.

II. MODEL

A. Bead-stick polymer model

The polymer chain is described by a coarse-grained off-lattice model for semiflexible homopolymers which has also been used for studies of heteropolymers in the frame of the hydrophobic-polar model [48]. As in lattice models, the adjacent monomers are connected by rigid covalent bonds. Thus, the distance is kept fixed and set to unity. The contact interaction of lattice models is replaced by a distance-dependent Lennard-Jones (LJ) potential accounting for short-range excluded volume repulsion and long-range interaction. An additional interaction accounts for the bending energy of any pair of successive bonds. The position vector of the ith monomer, $i = 1, \ldots, N$, is denoted by $\vec{r}_i$. A polymer with N monomers has $N-1$ bonds of length unity between neighboring monomers and $N-2$ bending angles ϑ_i, defined through

$$\cos\vartheta_i = (\vec{r}_{i+1} - \vec{r}_i) \cdot (\vec{r}_{i+2} - \vec{r}_{i+1}) \,. \tag{1}$$

The LJ potential of nonbonded monomers is of standard $12-6$ form. This model was first employed in two dimensions [48] and later generalized to three-dimensional AB proteins [49, 50], partially with modifications taking implicitly into account additional torsional energy contributions of each bond. The energy function for the polymer is thus given by

$$E_p \;=\; 4 \sum_{i=1}^{N-2} \sum_{j=i+2}^{N} \left(r_{ij}^{-12} - r_{ij}^{-6} \right) + \frac{1}{4} \sum_{i=1}^{N-2} \left(1 - \cos\vartheta_i \right) . \tag{2}$$

Note that the coupling of the bending energy is so weak that the polymer is almost flexible.

In this work, we assume that the polymer chain interacts with an attractive spherical surface. The interaction of the polymer chain monomers and the attractive sphere is modeled by the energy [43]

$$V_{\rm s} = 4\epsilon_c \frac{\pi R_{\rm s}}{r_i} \left\{ \frac{1}{5} \left[\left(\frac{\sigma}{r_i - R_{\rm s}} \right)^{10} - \left(\frac{\sigma}{r_i + R_{\rm s}} \right)^{10} \right] - \frac{\epsilon}{2} \left[\left(\frac{\sigma}{r_i - R_{\rm s}} \right)^{4} - \left(\frac{\sigma}{r_i + R_{\rm s}} \right)^{4} \right] \right\} , \tag{3}$$

where $R_{\rm s}$ is the radius of the sphere, $r_i = (x_i^2 + y_i^2 + z_i^2)^{1/2} \geq R_{\rm s}$ is the distance of a monomer to the origin and x_i, y_i, z_i are the coordinates of monomers, and σ, ϵ_c, and ϵ are set to unity. The radius of the sphere $R_{\rm s}$ is varied during the simulations. The functional dependence of the potential is shown in Fig. 1 for selected $R_{\rm s}$ values.

To make contact to experimental polymer-substrate systems one may identify the empirical (dimensionful) coupling parameters of, say, the Martini force field [51] with the (dimensionless) parameters of our coarse-grained model. For instance, from Table 1 in Ref. [52] we read off that methylene has $\epsilon_{\rm phys} = 104 \times 8.31/1000 = 0.86$KJ/mol which maps approximately onto $\epsilon = 1.0$ in our model. We obtain that the 20-mer (4 methylenes per bead) discussed in our model corresponds very approximately to n-C80. Similarly, the substrate maps approximately onto a polystyrene colloidal sphere, but its adsorption propensity is weaker than that of carbon or silica.

III. SIMULATION SETUP

A. Multicanonical method

In order to obtain statistical results of sufficient accuracy we applied the multicanonical Monte Carlo algorithm [53] (for reviews, see Refs. [54, 55]), where the energy distribution is flattened artificially allowing, in principle, for a

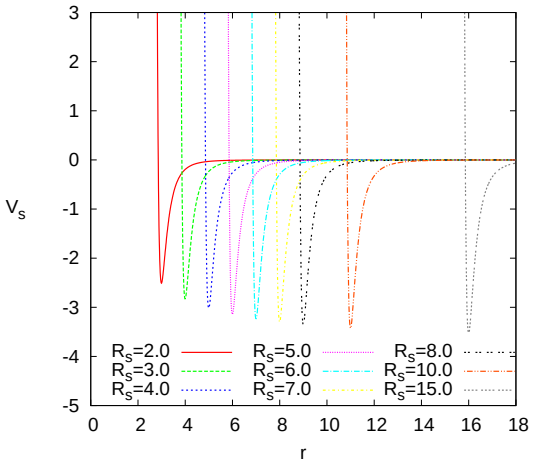

FIG. 1: The functional dependence of the attractive sphere potential (3) for different values of the sphere radius R_s.

random walk of successive states in energy space. This flattening is controllable and therefore reproducible. To this end, the Boltzmann probability is multiplied by a weight factor $W(E)$, which in our case is a function of the energy. Then the multicanonical probability for a state $\{\mathbf{x}\}$ with energy $E(\{\mathbf{x}\})$ reads $p_M(E) = \exp(-E/k_BT)W(E)$. In order to obtain a multicanonical or "flat" distribution, the initially unknown weight function $W(E)$ has to be determined iteratively: In the beginning, the weights $W^{(0)}(E)$ are set to unity for all energies letting the first run be a usual Metropolis simulation which yields an estimate $H^{(0)}(E)$ for the canonical distribution. This histogram is used to determine the next guess for the weights, the simplest update is to calculate $W^{(1)}(E) = W^{(0)}(E)/H^{(0)}(E)$. Then the next run is performed with probabilities $p_M^{(1)}(E) = \exp(-E/k_BT)W^{(1)}(E)$ of states with energy E, yielding $H^{(1)}(E)$ and $W^{(2)}(E) = W^{(1)}(E)/H^{(1)}(E)$, and so on. The iterative procedure is continued until the weights are appropriate in a way that the multicanonical histogram $H(E)$ is "flat". After having determined accurate weights $W(E)$, they are kept fixed and following some thermalization sweeps a long production run is performed, where statistical quantities O are obtained multicanonically, $\langle O\rangle_M = \sum_{\{\mathbf{x}\}} p_M(E(\{\mathbf{x}\}))O(\{\mathbf{x}\})/Z_M$ with the multicanonical partition function $Z_M = \sum_{\{\mathbf{x}\}} p_M(E(\{\mathbf{x}\}))$. The canonical statistics is obtained by reweighting the multicanonical to the canonical distribution, i.e., expectation values are computed as $\langle O\rangle = \langle OW^{-1}\rangle_M/\langle W^{-1}\rangle_M$. For a recent review of these methodological aspects in the context of polymer simulations, see Ref. [56].

B. Observables

To obtain as much information as possible about the canonical equilibrium behavior, we define the following suitable quantities O. Next to the canonical expectation values $\langle O\rangle$, we also determine the fluctuations about these averages, as represented by the temperature derivative $d\langle O\rangle/dT = (\langle OE\rangle - \langle O\rangle\langle E\rangle)/T^2$. We use generic units, in which $k_B = 1$.

In order to identify conformational transitions, the specific heat (per monomer) $C_V(T) = (\langle E^2\rangle - \langle E\rangle^2)/NT^2$ with $\langle E^k\rangle = \sum_E g(E)E^k \exp(-E/T)/\sum_E g(E)\exp(-E/T)$ is calculated from the density of states $g(E)$. The density of states was found (up to an unimportant overall normalization constant) by reweighting the multicanonical energy distribution obtained with multicanonical sampling to the canonical distribution. Details are given in Ref. [57].

Apart from the specific heat, several structural quantities are of interest. In order to check the structural compactness of conformations or to identify the possible dispersion of conformations because of adsorption, the radius of gyration of the conformations is calculated. The radius of gyration is a measure for the extension of the polymer and defined by $R_g^2 \equiv \sum_{i=1}^N (\vec{r}_i - \vec{r}_{cm})^2/N = \sum_{i=1}^N \sum_{j=1}^N (\vec{r}_i - \vec{r}_j)^2/2N^2$ with $\vec{r}_{cm} = \sum_{i=1}^N \vec{r}_i/N$ being the center-of-mass of the polymer.

We also calculated various shape descriptors derived from the gyration tensor [58–61] which is defined as

$$S = \frac{1}{N}\begin{pmatrix} \sum_i (x_i - x_{cm})^2 & \sum_i (x_i - x_{cm})(y_i - y_{cm}) & \sum_i (x_i - x_{cm})(z_i - z_{cm}) \\ \sum_i (x_i - x_{cm})(y_i - y_{cm}) & \sum_i (y_i - y_{cm})^2 & \sum_i (y_i - y_{cm})(z_i - z_{cm}) \\ \sum_i (x_i - x_{cm})(z_i - z_{cm}) & \sum_i (y_i - y_{cm})(z_i - z_{cm}) & \sum_i (z_i - z_{cm})^2 \end{pmatrix}. \quad (4)$$

Transformation to the principal axis system diagonalizes S,

$$S = \mathrm{diag}(\lambda_1, \lambda_2, \lambda_3), \quad (5)$$

where we assume that the eigenvalues of S are sorted in descending order, i.e., $\lambda_1 \geq \lambda_2 \geq \lambda_3$. The first invariant of S gives the squared radius of gyration,

$$\mathrm{Tr}\, S = \lambda_1 + \lambda_2 + \lambda_3 = R_g^2, \tag{6}$$

which agrees with the definition given above. The second invariant shape descriptor, or relative shape anisotropy, is defined as

$$\kappa^2 \equiv A_3 = \frac{3}{2}\frac{\mathrm{Tr}\hat{S}^2}{(\mathrm{Tr}S)^2} = 1 - 3\frac{\lambda_1\lambda_2 + \lambda_2\lambda_3 + \lambda_3\lambda_1}{(\lambda_1 + \lambda_2 + \lambda_3)^2}, \tag{7}$$

where $\hat{S} = S - \frac{1}{3}(\mathrm{Tr}S)E$ with unit tensor E. It reflects both the symmetry and dimensionality of a polymer conformation. This parameter is limited between the values of 0 and 1. It reaches 1 for an ideal linear chain and drops to zero for highly symmetric conformations. For planar symmetric objects, the relative shape anisotropy converges to the value of 1/4 [58–62].

The distance of the center-of-mass, r_{cm}, of the polymer to the surface also provides clear evidence that the polymer is freely moving or that it is very close to the surface and just adsorbed. Another useful quantity is the mean number of monomers $\langle N_s \rangle$ docked to the surface. A single-layer structure is formed if all monomers are attached at the sphere; if none is attached, the polymer is desorbed. The sphere potential is a continuous potential, and in order to distinguish monomers docked to the sphere from those not being docked, it is reasonable to introduce a cutoff. We define a monomer i as being "docked" if $r_i - R_s < r_c \equiv 1.2$. The corresponding measured quantity is the average number $\langle N_s \rangle$ of monomers docked to the surface. This can be expressed as $N_s = \sum_{i=1}^{N} \Theta(r_c - r_i)$, where $\Theta(r)$ is the Heaviside step function.

C. Computational details

In our simulations, the polymer chain length is $N = 20$ and we set $\epsilon = 1.0$ large enough to allow adsorption of the polymer to the sphere surface. We consider two different situations, one is the case where the polymer is grafted with one end to the substrate and in the second case it is allowed to move freely in the space above the substrate over a distance $L = 60 - R_{\mathrm{s}}$ from the sphere surface (i.e., the nano-sphere of radius R_{s} is centered in a spherical container

FIG. 2: (Color online) Start configurations of the simulations: (a) non-grafted, (b) end-grafted.

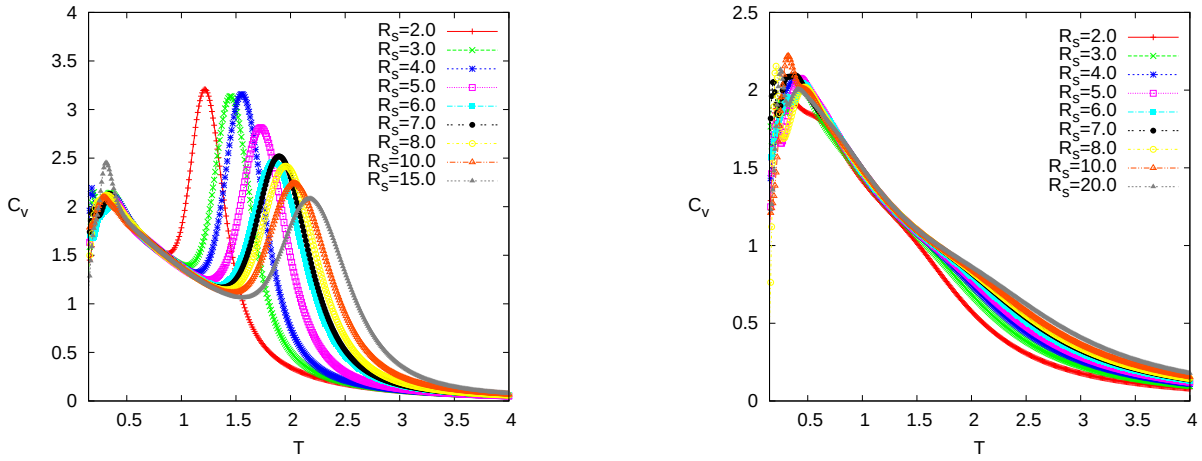

(a) (b)

FIG. 3: (Color online) Specific heat as a function of temperature for different sphere radii R_s for the (a) non-grafted and (b) end-grafted case.

of radius 60 with a purely steric wall), which is called the free or non-grafted case. We have done simulations with different sizes of the sphere. The random initial configurations for the non-grafted and grafted cases of the simulation are sketched in Figs. 2(a) and (b). The total energy of the system is composed of the pure polymer chain energy and the polymer chain attractive sphere interaction energy. The initial configuration of the polymer chain is randomly generated. For the determination of the multicanonical weights we performed 200 iterations with at least 10^5 sweeps each. In the production period, 1×10^8 sweeps were generated to have reasonable statistics for estimating the thermodynamic quantities. Statistical errors are estimated with the standard Jackknife technique [63–65].

IV. RESULTS

A. Energetic fluctuations

In Fig. 3 the specific-heat curves $C_V(T)$ as a function of temperature T for different values of sphere radius R_s are displayed for the (a) non-grafted and (b) end-grafted case. The specific heat shows two transitions for both cases: one is the low-temperature transition which is almost at the same temperature for all different R_s values. This is the freezing transition. Even though this transition occurs at the same temperature, the conformations have different characteristic shapes depending on the attraction strength of the sphere. For describing these different shapes we will concentrate on structural observables to be discussed below. The second transition has only a weak signal for the grafted case (a shoulder at $T \approx 2.0$) but for the non-grafted case it is quite pronounced. This is the adsorption transition, which comes into play at higher temperatures than the freezing transition and depends on the sphere radius. Increasing the sphere radius causes also an increase in the adsorption transition temperature. This transition separates desorbed (D) and adsorbed (A) conformations.

B. Phase diagram

The phase structure derived from all of our observables is summarized by the phase diagrams in the $R_s - T$ plane given in Fig. 4 for the (a) non-grafted and (b) end-grafted case. Representative conformations that predominate in the different structural phases are revealed in Fig. 5. The phase diagram is constructed by combining all the informations coming from the canonical expectation values of our observables and their temperature derivatives. Some of our observables exhibit a peak at all of the transitions in the phase diagram, while others are only sensitive to one of them. For example, the collapse transition line is seen quite clearly from the peak in the temperature derivative of the canonical expectation value of the eigenvalues of the gyration tensor and from the radius of gyration. On the other hand, the adsorption line is most clearly built up by the mean number of adsorbed monomers to the surface

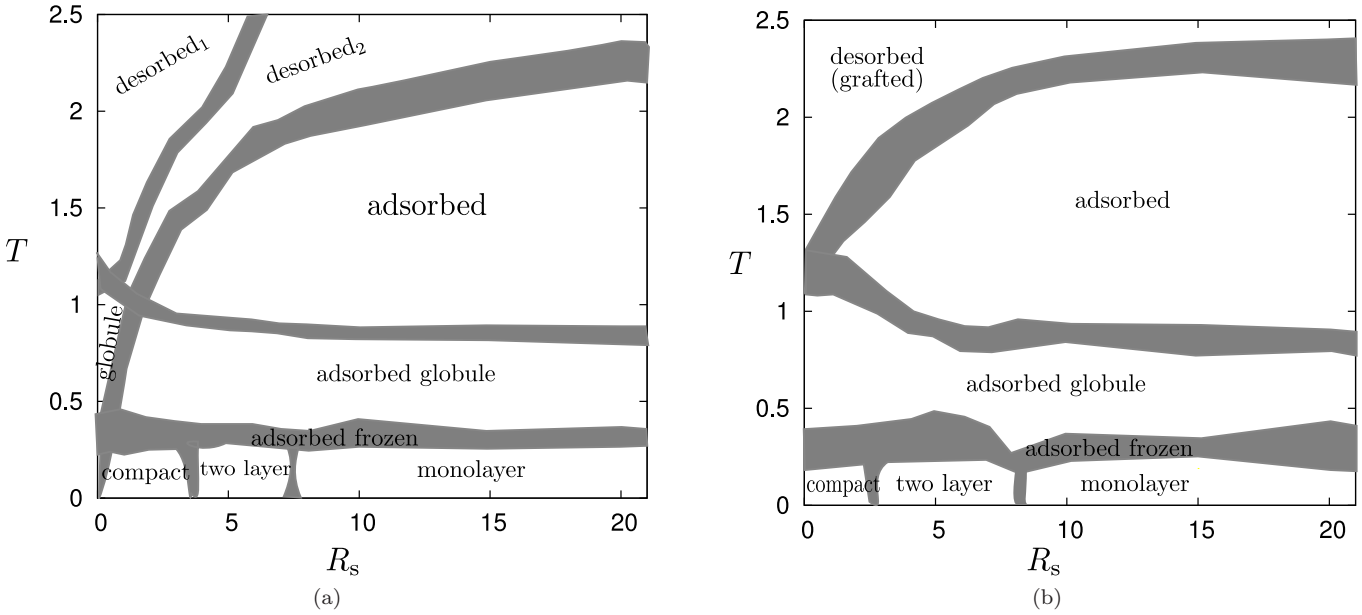

FIG. 4: The phase diagram of the homopolymer-attractive spherical surface system for a (a) non-grafted and (b) end-grafted polymer as obtained in extensive multicanonical simulations. The boundaries separate the individual conformational phases. The band width shows the variation of the peaks of temperature derivatives of different structural observables which have been analyzed simultaneously.

and by the distance of the center-of-mass of the polymer to the substrate. Since our system is a finite system, it is not possible to determine the transition lines precisely: The transition lines still vary with chain length N and the observables have broad peaks. Thus we have a certain band width which approximately covers the different peaks in the observables.

In the phase diagram the temperature increases from bottom to top and the radius of the sphere increases from left to right. The boundaries separate the individual conformational phases. For small sphere radius R_s, the polymer behaves similarly to a free polymer where at high temperatures the typical conformations are desorbed and extended or random coil. Decreasing the temperature causes the collapse transition into globular conformations which are still in the desorbed phase. But below the freezing transition all the compact conformations are adsorbed. At this point, for the grafted case all the conformations are already adsorbed below the collapse transition. There is no desorbed globule phase in the grafted phase diagram. One more difference occurred also in the high-temperature desorbed phase. In the non-grafted case some structural observables give indication for some changes in the desorbed phase. When we detect carefully the conformations we see that those in the "desorbed$_1$" phase are far away from the sphere surface while the conformations in the "desorbed$_2$" phase are almost adsorbed. Thus they feel very strongly the surface effect. Because of the grafting, this is not the case for a grafted polymer. Increasing the sphere radius approximately to $R_s = 7.0$ leads to very fast increase in the adsorption transition temperature, but after this value it increases slowly. The adsorption transition separates the regions of desorbed and adsorbed phases. Besides the collapse, adsorption, and freezing transitions, the most pronounced transition is the layering transition which occurs at $R_s \approx 7.0$ and separates the region of planar conformations which are monolayers and totally adsorbed conformations from the two-layer and compact conformations.

In the following discussion we will mainly focus on the non-grafted polymer and display the findings from the structural observables in detail only for this case. However, since the phase diagrams in Figs. 4(a) and (b) rely on these data, we have measured and analyzed all these observables for the grafted case, too, and hence shall give at least an overview of the analogous results in a panel of figures at the end of this section, but refrain from a detailed description.

C. Structural parameters and fluctuations

In Figs. 6(a) and (b), the radius of gyration $\langle R_g \rangle$ as a function of temperature and its temperature derivative $d\langle R_g \rangle / dT$ are given for different values of the sphere radius R_s, respectively. For small values of R_s, $R_s = 0.5, 1.0,$

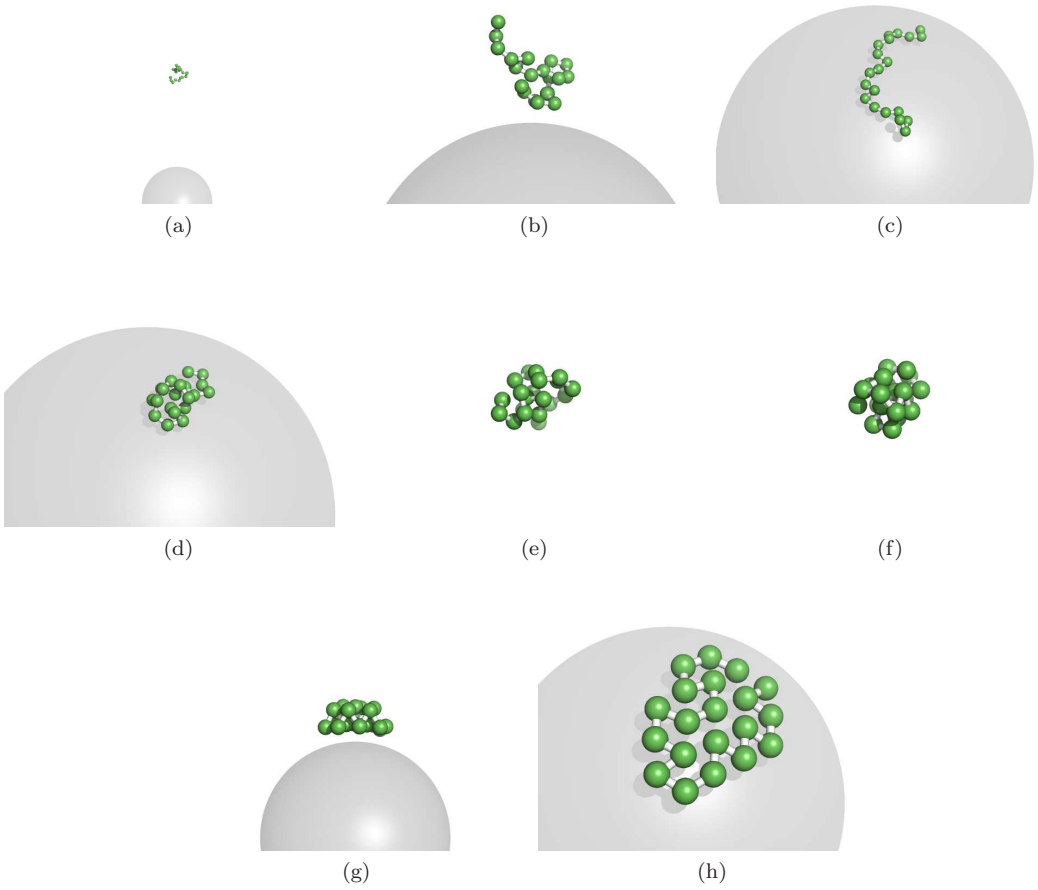

FIG. 5: (Color online) Typical conformations for the regions (a) desorbed$_1$, (b) desorbed$_2$, (c) adsorbed, (d) adsorbed globule, (e) globule, (f) compact, (g) two layer, and (h) monolayer in the phase diagram.

the most compact conformations occur in the low-temperature region with an average $\langle R_g \rangle \approx 1.23$ (data not shown). Slightly increasing the R_s value causes also an increase in the average $\langle R_g \rangle$ value to about 1.4. Increasing the R_s parameter further, the curve at $R_\mathrm{s} = 7.0$ has a minimum behavior at low temperatures. As a function of temperature the radius of gyration is monotonically increasing for all R_s values except beyond $R_\mathrm{s} = 7.0$ where the layering transition occurs. Same supporting informations are also gained from the relative shape anisotropy parameter which is shown in Fig. 7.

If we consider now the temperature derivative given in Fig. 6(b), we detect two peaks. The peak in the temperature derivative of the canonical expectation value of radius of gyration at low temperatures indicates the collapse transition quite clearly. Also its tensor eigenvalues [Figs. 10(a) and (b) below] and particularly the relative shape anisotropy parameter $\langle \kappa^2 \rangle$ in Figs. 7(a) and (b), which is the second invariant of the tensor, give rich information and support our findings. As we discussed before the desorbed phase is divided into two regions which are called "desorbed$_1$" and "desorbed$_2$". The boundary of these regions is emerging in the temperature derivative of radius of gyration $d\langle R_g \rangle / dT$ and in the temperature derivative of the relative shape anisotropy $d\langle \kappa^2 \rangle / dT$ as a second peak at high temperatures, since the peaks are going to become invisible with increasing R_s values and also are smaller than the peaks at low temperatures. We have investigated the conformations in both regions in detail and concluded that the conformations in the "desorbed$_1$" phase are far away from the surface. On the other hand, the conformations in the "desorbed$_2$" phase are almost adsorbed to the sphere boundary, which indicates the influence of the surface on the desorbed phase.

The adsorption transition can best be detected by the distance of the center-of-mass of the polymer to the substrate r_cm and by the mean number of adsorbed monomers, where a monomer is defined to be adsorbed to the surface if $r_i - R_\mathrm{s} < 1.2$. The behavior of these two observables, in particular the peaks in their temperature derivatives, build the adsorption line in the phase diagrams. In Figs. 8(a) and (b) the distance of the center-of-mass of the polymer to the substrate and its temperature derivative are given, respectively. As can be seen in the figure, for large temperatures

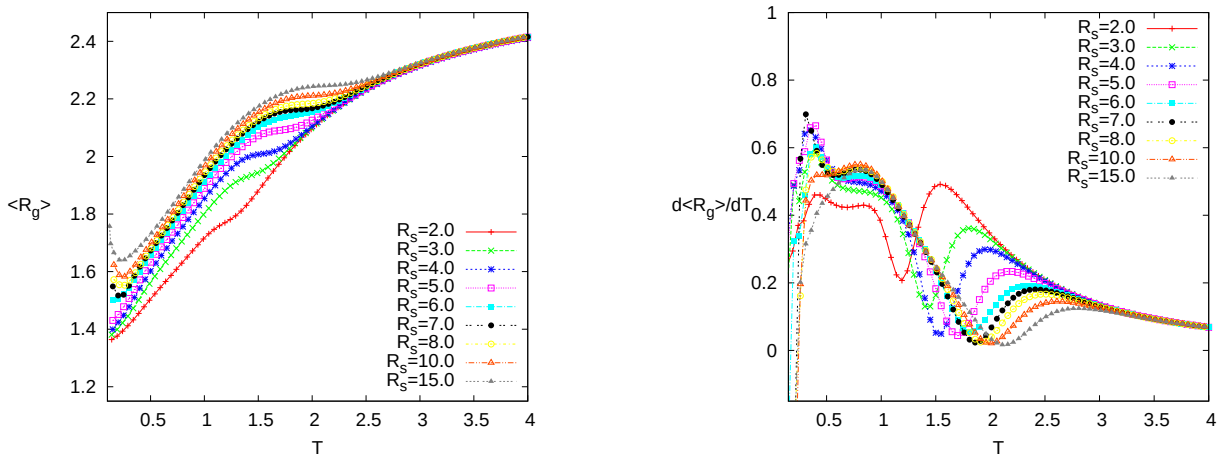

(a) (b)

FIG. 6: (Color online) (a) The canonical expectation value of the radius of gyration $\langle R_g \rangle$ and (b) its temperature derivative for different sphere radii R_s.

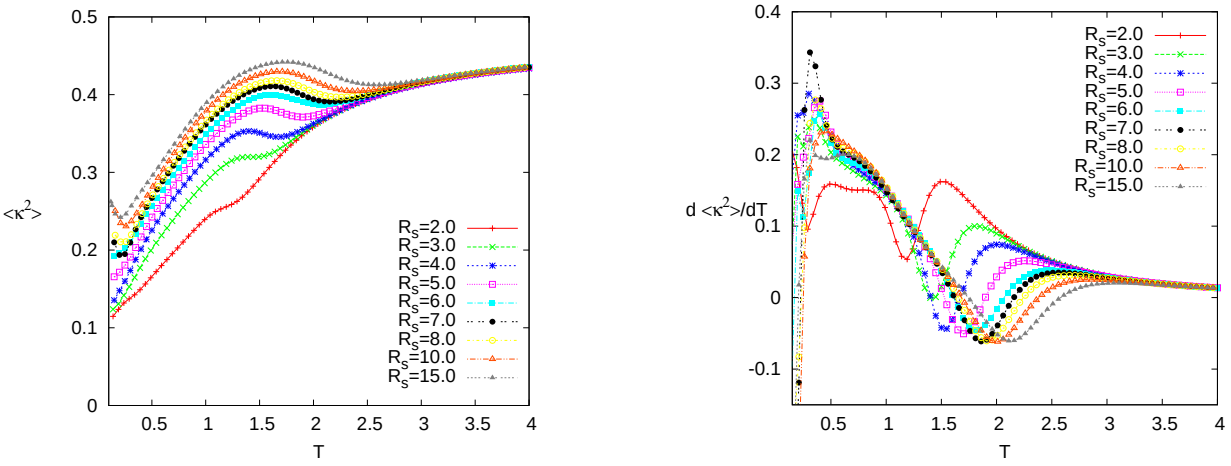

(a) (b)

FIG. 7: (Color online) (a) The canonical expectation value of the relative shape anisotropy parameter $\langle \kappa^2 \rangle$ and (b) its temperature derivative for different sphere radii R_s.

the polymer can move freely within the simulation space and the influence of the surface is minimal only for high R_s values, whereas for low R_s the influence is purely steric. Thus, the average center-of-mass distance of the polymer above the surface is nearly half of the simulation space. On contrary, at low temperatures the polymer favors surface contacts and the average center-of-mass distance converges to the minimum location of the potential (cf. Fig. 1). One clearly detects a quite pronounced peak in its temperature derivative [Fig. 8(b)] that divides the phase space into adsorbed and desorbed phases. Consistently with our discussion above, the pronounced tendency of the polymer to make surface contacts can be also identified from the mean number of adsorbed monomers to the surface $\langle N_s \rangle$ [Fig. 9(a)] and the negative minima in its temperature derivative [Fig. 9(b)]. They are in good agreement with the sharp peaks in the temperature derivative of the distance of the center-of-mass of the polymer which together draws the adsorption line in the phase diagram.

Finally, the eigenvalues of the gyration tensor which measure the extensions in the principle axis system are extracted to complement the picture. In Figs. 10(a)-(f) the eigenvalues of the gyration tensor and their fluctuations as a function of temperature T for different values of R_s are displayed. They all support our earlier findings. But the most important result deductible from the eigenvalues is that: The third eigenvalue of the gyration tensor $\langle \lambda_3 \rangle$ converges to small values which means that the extension in the third direction vanishes and the conformations are two-dimensional signaling the layering transition. To support this finding one can also plot the ratio of the largest

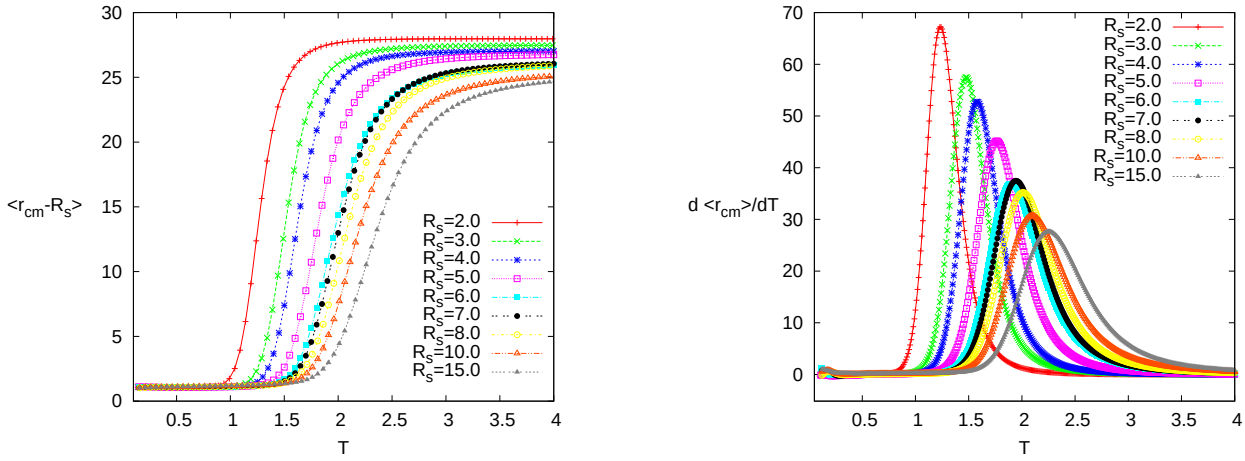

(a) (b)

FIG. 8: (Color online) (a) The canonical expectation value of the distance of the center-of-mass of the polymer $\langle r_{\rm cm}\rangle$ from the sphere surface and (b) its temperature derivative for different sphere radii $R_{\rm s}$.

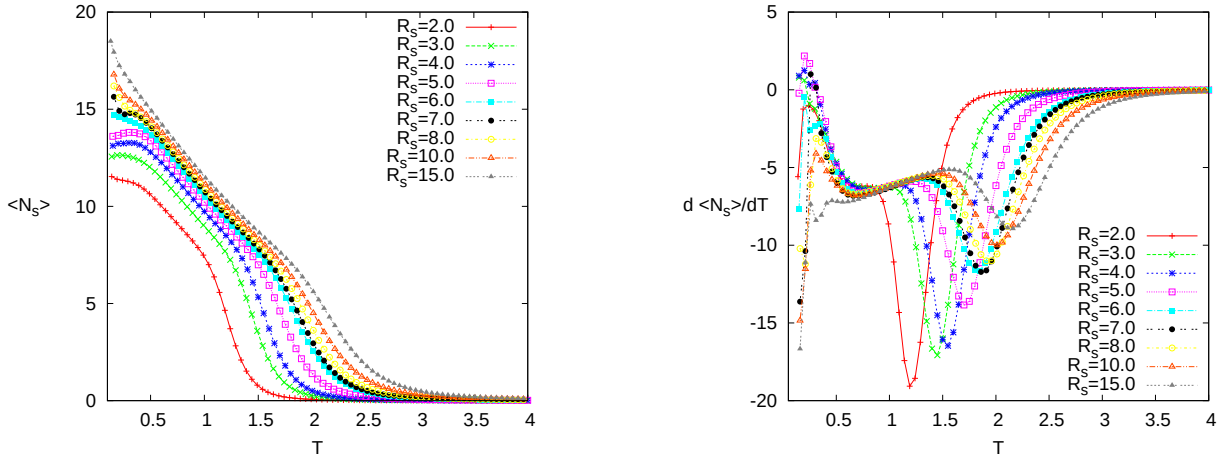

(a) (b)

FIG. 9: (Color online) (a) The canonical expectation value of the mean number of docked monomers $\langle N_s\rangle$ and (b) its temperature derivative for different sphere radii $R_{\rm s}$.

eigenvalue to the smallest eigenvalue $\langle\lambda_1/\lambda_3\rangle$ and its temperature derivative as in Fig. 11. This ratio assumes small values until $R_{\rm s}\approx 7.0$. Above $R_{\rm s}=7.0$ the ratio of the eigenvalues jumps to much higher values, signaling that the layering transition occurs at this $R_{\rm s}$ value and separates the conformational space from planar conformations.

D. Grafted case

Finally, for comparison we show for the grafted case in Figs. 12(a)-(h) the analogs to Figs. 6-9. These results are used when constructing the phase diagram for an end-grafted polymer in Fig. 4(b). By comparing this set of plots with the free case, the most important outcome is that: A crossover occurs from low temperature, where the polymer is adsorbed and the conformations of a grafted polymer and a free polymer are very similar, to high temperatures, where the free polymer approaches the behavior of a polymer in bulk solution while that of a grafted polymer is always affected by the attractive sphere surface. Because of this effect, the transition is just a crossover which can be clearly seen in the $\langle r_{\rm cm}\rangle$ and $\langle N_s\rangle$ parameters. In the free case these parameters change sharply because as soon as the polymer desorbs, it leaves the influence of the surface field. A grafted polymer, on the other hand, cannot leave the surface field. The freezing transition, however, signaled by the low-temperature peak in the specific heat displayed

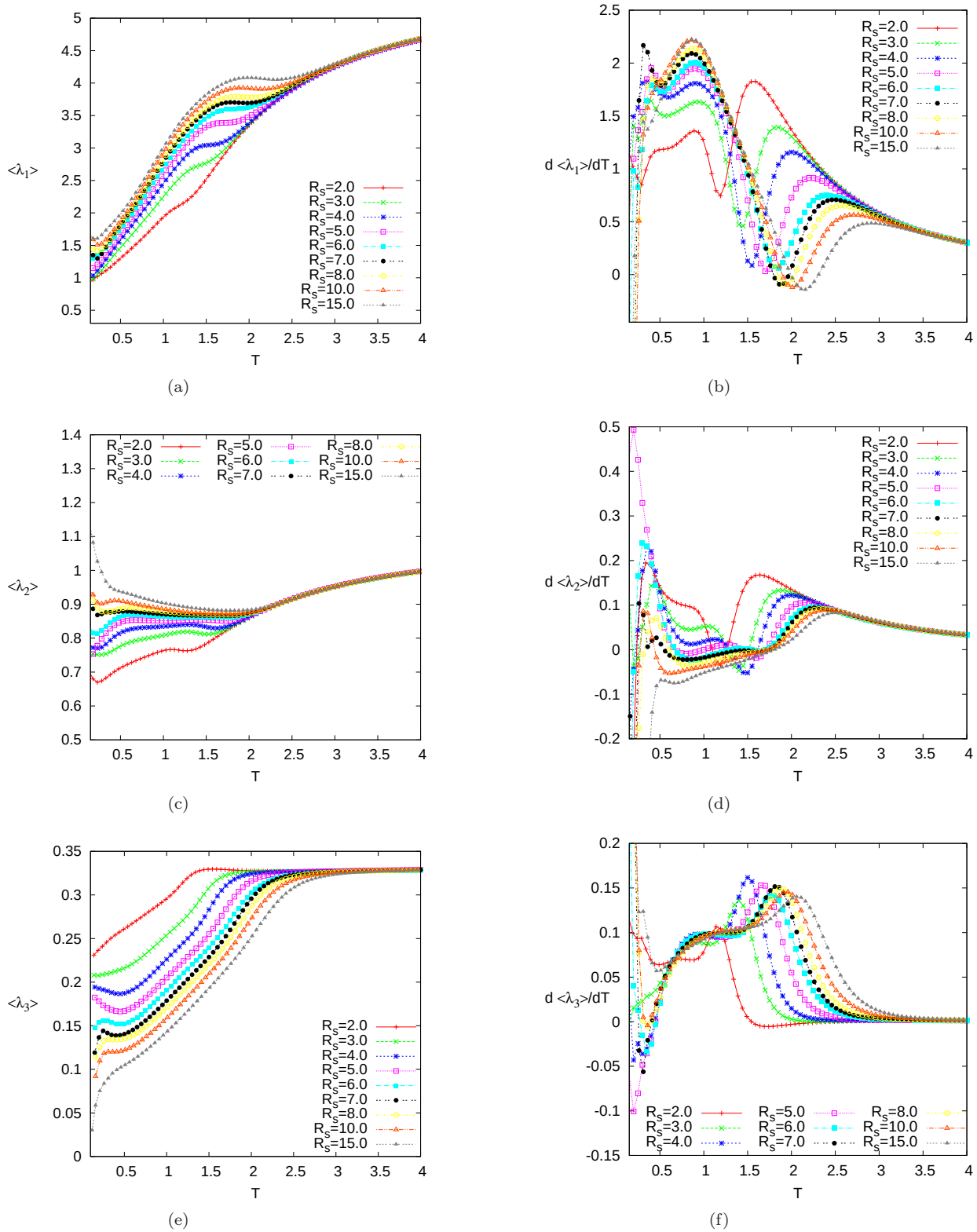

FIG. 10: (Color online) The canonical expectation values of the three eigenvalues $\langle\lambda_1\rangle$, $\langle\lambda_2\rangle$, and $\langle\lambda_3\rangle$ of the gyration tensor and their temperature derivatives for different sphere radii R_s.

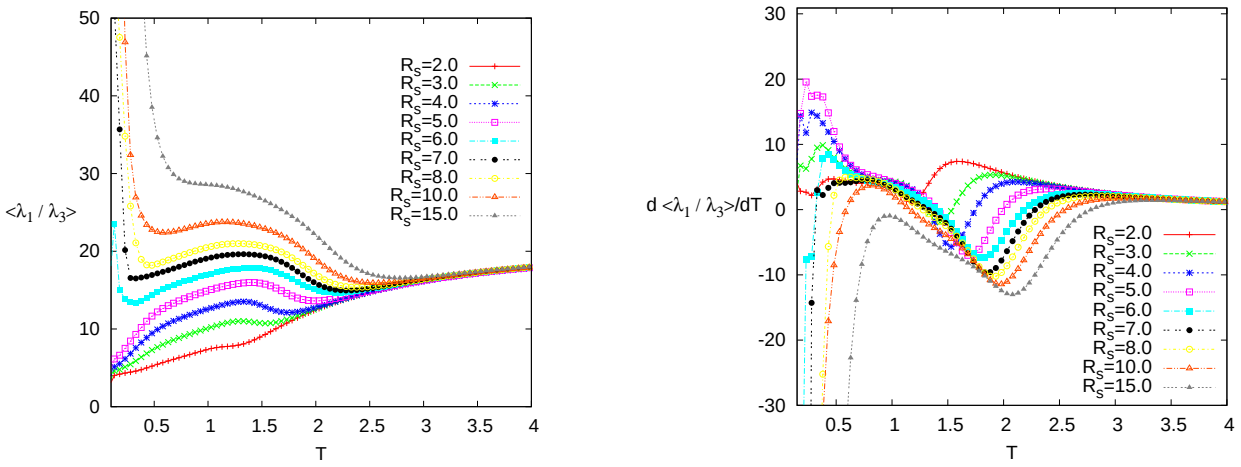

(a) (b)

FIG. 11: (Color online) (a) The ratio of the largest eigenvalue to the smallest eigenvalue $\langle\lambda_1/\lambda_3\rangle$ and (b) its temperature derivative for different sphere radii R_s.

in Fig. 3(b), does not differ much for grafted and non-grafted chains.

V. CONCLUSION

In this paper, we have performed generalized-ensemble Monte Carlo computer simulations in order to investigate the full conformational behavior of a coarse-grained semiflexible finite polymer chain near an attractive spherical surface. In a systematic analysis, over a wide range of sphere radius R_s and temperature T, we have constructed the phase diagrams both for non-grafted and end-grafted polymers. For the identification of the conformational phases, we have examined several energetic and structural observables and their fluctuations by canonical statistical analysis. The transition lines in the phase diagram show the best match of all observables analyzed simultaneously in our study. In the thermodynamic limit of infinitely long chains the transitions are expected to occur at sharp values of the parameters. For finite chains, the transition lines still vary with chain length N and are not well defined because of broad peaks in the observables that also have small differences in between. Therefore the locations of the phase boundaries should be considered as a rough guide. However, even for the rather short chains considered here, we can clearly identify different phases which show distinguishing features, so that a reasonable picture is obtained. Most of the phases are believed to still persist for longer chains. All our results obtained from the different observables are summarized in the phase diagrams in the $R_s - T$ plane which for a convenient overview were already displayed earlier in Figs. 4(a) for non-grafted and (b) for end-grafted polymers. Their typical conformations were also revealed already earlier in Fig. 5. To summarize these findings, we give in the following a short description of each phase:

Desorbed$_1$: Random coil structures with no surface contacts. These conformations freely circulate in the simulation space and are far away from the surface of the sphere [Fig. 5(a)].

Desorbed$_2$: Desorbed conformations, but they are almost adsorbed. The conformations feel the influence of the surface [Fig. 5(b)].

Adsorbed: Partially adsorbed, extended conformations [Fig. 5(c)].

Adsorbed Globule: Partially adsorbed conformations [Fig. 5(d)].

Globule: Desorbed globule conformations. These conformations are only seen on the non-grafted phase diagram [Fig. 5(e)].

Compact: Partially adsorbed, globular conformations like a drop on the wall of the sphere [Fig. 5(f)].

Two Layer: Partially adsorbed, compact conformations. These are two-layer structures. The lower layer of the conformations is adsorbed and lies on the wall of the sphere [Fig. 5(g)].

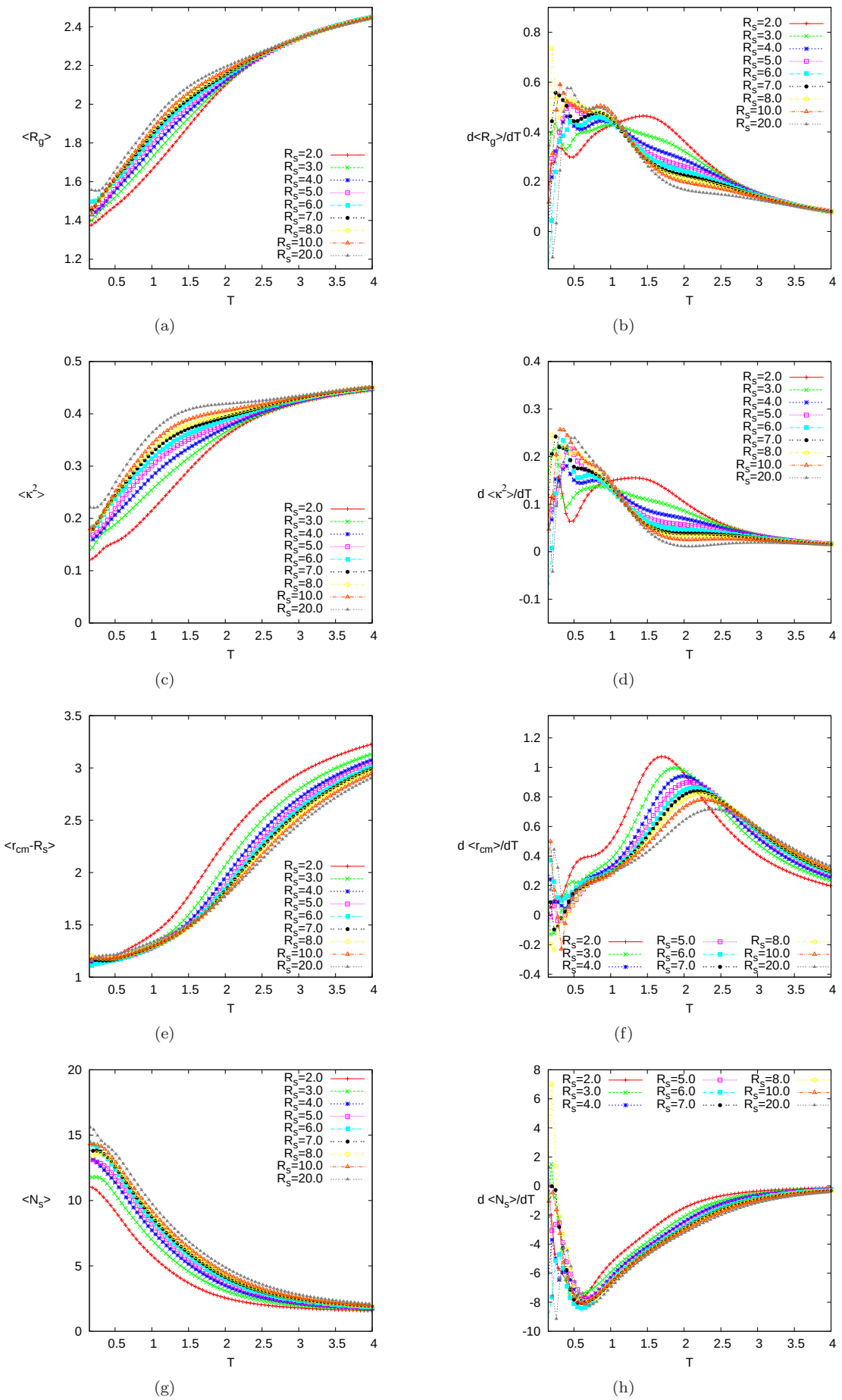

FIG. 12: (Color online) Same observables as in Figs. 6-9 but here for the end-grafted case.

Monolayer: Completely adsorbed, compact conformations. These single-layer structures lie on the surface of the sphere and fit the sphere wall perfectly [Fig. 5(h)].

It is clear that, for longer chains, the desorbed, globule and compact phases obviously will survive. Additionally, filmlike (monolayer) and semispherical conformations (two layer), as well as surface attached globular shapes will dominate the respective phases. On the other hand, as long as surface effects are as influential as volume effects the compact adsorbed conformations differ noticeably for polymers with different but small lengths. But, for the majority of phases we find qualitative coincidence with a simple coarse-grained model.

In addition to experimental results [66, 67], Feng and Ruckenstein [34] examined the adsorption of a polyampholyte chain on a single spherical nano-particle with three different radii of the particles. There, the charge density at the particle surface regulates the strength of the adsorption field and the polymer composition regulates the location of the coil-globule transition. In this study, we kept the adsorption field constant (whereas we varied the adsorption strength in another earlier study) and varied the radius of the nano-particles and observed qualitatively the described scenarios. As a result, our model system can be mapped in the considered parameter range to a real system considered in experiments. Comparing with experimental findings, computational studies have the advantage that different combinations of parameters can be varied at will over long ranges and a deeper knowledge starting from the origin can be extracted.

ACKNOWLEDGMENTS

We wish to thank Viktoria Blavatska and Bernd Abel for useful discussions. H.A. acknowledges support by the Alexander von Humboldt Foundation under the Experienced Researcher Fellowship Programme. W.J. thanks the German Research Foundation (DFG) for support under Grant Nos. JA483/24-3 and SFB/TRR 102 (Project B04). We also benefitted from the Marie Curie IRSES network DIONICOS under Contract No. PIRSES-GA-2013-612707 within the European Union Seventh Framework Programme. The computer time for the Monte Carlo simulations was provided by NIC, Forschungszentrum Jülich, under Grant No. hlz21, which we gratefully acknowledge.

[1] R. F. Service, Science **270**, 230 (1995).
[2] S. Walheim, E. Schaffer, J. Mlynek, and U. Steiner, Science **283**, 520 (1999).
[3] S. Brown, Nature Biotechn. **15**, 269 (1997).
[4] R. Braun, M. Sarikaya, and K. Schulten, J. Biomater. Sci. Polymer Edn. **13**, 747 (2002).
[5] S. R. Whaley, D. S. English, E. L. Hu, P. F. Barbara, and A. M. Belcher, Nature **405**, 665 (2000).
[6] K. Goede, P. Busch, and M. Grundmann, Nano Lett. **4**, 2115 (2004).
[7] M. Bachmann, K. Goede, A. G. Beck-Sickinger, M. Grundmann, A. Irbäck, and W. Janke, Angew. Chem. Int. Ed. **49**, 9530 (2010).
[8] E. Eisenriegler, K. Kremer, and K. Binder, J. Chem. Phys. **77**, 6296 (1982).
[9] R. Descas, J.-U. Sommer, and A. Blumen, J. Chem. Phys. **120**, 8831 (2004).
[10] M. Bachmann and W. Janke, Phys. Rev. Lett. **95**, 058102 (2005).
[11] M. Bachmann and W. Janke, Phys. Rev. E **73**, 020901(R) (2006).
[12] M. Bachmann and W. Janke, Phys. Rev. E **73**, 041802 (2006).
[13] J. Luettmer-Strathmann, F. Rampf, W. Paul, and K. Binder, J. Chem. Phys. **128**, 064903 (2008).
[14] M. Bachmann and W. Janke, in: *Rugged Free Energy Landscapes: Common Computational Approaches to Spin Glasses, Structural Glasses and Biological Macromolecules*, ed. W. Janke, Lect. Notes Phys. **736** (Springer, Berlin, 2008); pp. 203–246.
[15] M. Möddel, M. Bachmann, and W. Janke, J. Phys. Chem. B **113**, 3314 (2009).
[16] V. A. Ivanov, J. A. Martemyanova, M. Müller, W. Paul, and K. Binder, J. Phys. Chem. B **113**, 3653 (2009).
[17] T. Chen, L. Wang, X. Lin, Y. Liu, and H. Liang, J. Chem. Phys. **130**, 244905 (2009).
[18] L. Wang, T. Chen, X. Lin, Y. Liu, and H. Liang, J. Chem. Phys. **131**, 244902 (2009).
[19] A. D. Swetnam and M. P. Allen, Phys. Chem. Chem. Phys. **11**, 2046 (2009).
[20] M. Möddel, W. Janke, and M. Bachmann, Phys. Chem. Chem. Phys. **12**, 11548 (2010).
[21] M. Möddel, W. Janke, and M. Bachmann, Macromolecules **44**, 9013 (2011).
[22] Y. W. Li, T. Wüst, and D. P. Landau, Phys. Rev. E **87**, 012706 (2013).
[23] M. Möddel, W. Janke, and M. Bachmann, Phys. Rev. Lett. **112**, 148303 (2014).
[24] M. P. Taylor and J. Luettmer-Strathmann, J. Chem. Phys. **141**, 204906 (2014).
[25] J. Krawczyk, A. L. Owczarek, T. Prellberg, and A. Rechnitzer, J. Stat. Mech.: Theory Exp., P05008 (2005).
[26] S. Bhattacharya, V. G. Rostiashvili, A. Milchev, and T. A. Vilgis, Phys. Rev. E **79**, 030802(R) (2009).
[27] M. J. Russell, Science **302**, 580 (2003).

[28] M. Lundqvist, P. Nygren, B.-H. Jonsson, and K. Broo, Angew. Chem. Int. Ed. **45**, 8169 (2006).
[29] I. Gurevitch and S. Srebnik, Chem. Phys. Lett. **444**, 96 (2007); J. Chem. Phys. **128**, 144901 (2008).
[30] T. Vogel and M. Bachmann, Phys. Rev. Lett. **104**, 198302 (2010).
[31] T. Vogel, J. Gross, and M. Bachmann, J. Chem. Phys. **142**, 104901 (2015).
[32] R. R. Netz and J. F. Joanny, Macromolecules **31**, 5123 (1998).
[33] M. Tanaka, A. Yu Grosberg, and T. Tanaka, J. Chem. Phys. **110**, 8176 (1999); M. Tanaka and T. Tanaka, Phys. Rev. E **62**, 3803 (2000).
[34] J. Feng and E. Ruckenstein, Polymer **44**, 3141 (2003).
[35] M. Tagliazucchi, M. Olvera de la Cruz, and I. Szleifer, Proc. Natl. Acad. Sci. U.S.A. **107**, 5300 (2010).
[36] S. A. Barr and A. Z. Panagiotopoulos, J. Chem. Phys. **137**, 144704 (2012).
[37] A. Gladytz, M. Wagner, T. Häupl, C. Elsner, and B. Abel, Part. Part. Syst. Char. **32**, 573 (2015).
[38] C. Elsner, D. Hintzen, A. Prager, K. R. Siefermann, and B. Abel, Z. Phys. Chem. **229**, 427 (2015).
[39] M. Marenz, J. Zierenberg, H. Arkın, and W. Janke, Condens. Matter Phys. **15**, 43008 (2012).
[40] H. Arkın and W. Janke, Phys. Rev. E **85**, 051802 (2012).
[41] H. Arkın and W. Janke, J. Chem. Phys. **138**, 054904 (2013).
[42] H. Arkın and W. Janke, J. Phys. Chem. B **116**, 10379 (2012).
[43] H. Arkın and W. Janke, Eur. Phys. J. – Special Topics **216**, 181 (2013).
[44] T. Bogner, A. Degenhard, and F. Schmid, Phys. Rev. Lett. **93**, 268108 (2004).
[45] E. Balog, T. Becker, M. Oettl, R. Lechner, R. Daniel, J. Finney, and J. C. Smith, Phys. Rev. Lett. **93**, 028103 (2004).
[46] M. Ikeguchi, J. Ueno, M. Sato, and A. Kidera, Phys. Rev. Lett. **94**, 078102 (2005).
[47] N. Gupta and A. Irbäck, J. Chem. Phys. **120**, 3983 (2004).
[48] F. H. Stillinger, T. Head-Gordon, and C. L. Hirshfeld, Phys. Rev. E **48**, 1469 (1993); F. H. Stillinger and T. Head-Gordon, Phys. Rev. E **52**, 2872 (1995).
[49] A. Irbäck, C. Peterson, F. Potthast, and O. Sommelius, J. Chem. Phys. **107**, 273 (1997).
[50] A. Irbäck, C. Peterson, and F. Potthast, Phys. Rev. E **55**, 860 (1997).
[51] S. J. Marrink, H. J. Risselada, S. Yefimov, D. P. Tieleman, and A. H. de Vries, J. Phys. Chem. B **111**, 7812 (2007).
[52] A. L. Rodriguez, C. Vega, and J. J. Freire, J. Chem. Phys. **111**, 438 (1999).
[53] B. A. Berg and T. Neuhaus, Phys. Lett. B **267**, 249 (1991); Phys. Rev. Lett. **68**, 9 (1992); W. Janke, Int. J. Mod. Phys. C **3**, 1137 (1992).
[54] B. A. Berg, Fields Institute Communications **28**, 1 (2000).
[55] W. Janke, Physica A **254**, 164 (1998); and in: *Computer Simulations of Surfaces and Interfaces*, NATO Science Series, II. Mathematics, Physics and Chemistry – Vol. **114**, edited by B. Dünweg, D. P. Landau, and A. I. Milchev (Kluwer, Dordrecht, 2003), pp. 137–157.
[56] W. Janke and W. Paul, invited review, Soft Matter **12**, 642 (2016).
[57] M. Bachmann, H. Arkın, and W. Janke, Phys. Rev. E **71**, 031906 (2005).
[58] K. Solc and W. H. Stockmayer, J. Chem. Phys. **54**, 2756 (1971).
[59] D. N. Theodorou and U. W. Suter, Macromolecules **18**, 1206 (1985).
[60] V. Blavatska and W. Janke, J. Chem. Phys. **133**, 184903 (2010).
[61] J. Vymětal and J. Vondrášek, J. Phys. Chem. A **115**, 11455 (2011).
[62] V. Blavatska and W. Janke, J. Chem. Phys. **136**, 104907 (2012).
[63] B. Efron, *The Jackknife, the Bootstrap and Other Resampling Plans* (Society for Industrial and Applied Mathematics [SIAM], Philadelphia, 1982).
[64] W. Janke, *Monte Carlo methods in classical statistical physics*, in: *Computational Many-Particle Physics*, Wilhelm & Else Heraeus Summerschool, Greifswald, edited by H. Fehske, R. Schneider, and A. Weiße, Lect. Notes Phys. **739** (Springer, Berlin, 2008), pp. 79–140.
[65] W. Janke, *Monte Carlo simulations in statistical physics – From basic principles to advanced applications*, in: *Order, Disorder and Criticality: Advanced Problems of Phase Transition Theory*, Vol. 3, edited by Y. Holovatch (World Scientific, Singapore, 2012), pp. 93–166.
[66] V. Lesins and E. Ruckenstein, Colloid Polym. Sci. **266**, 1187 (1988).
[67] V. Lesins and E. Ruckenstein, J. Colloid Interface Sci. **132**, 566 (1989).